as the nonmatch. A new set of novel stimuli was used for each cell, and a given set was reused, if at all, no sooner than several months later. The nonmatching items used on each trial were chosen from a set of four different, already highly familiar, stimuli. A given sample stimulus was repeated in the session after 4 or 35 intervening trials with the other sample stimuli, the 4- and 35-trial intervals being used in alternation. About 200 to 400 trials, or 10 to 20 trials per sample stimulus, were typically used in each session.

For many IT neurons, the response to the initially novel sample stimuli systematically declined over the session as the animal gained more experience with them. Over one-third of the 72 neurons tested exhibited a significant decrease in response with repeated presentation of these stimuli (*9*) (Fig. 3), the amount of the decrement increasing across trials, reaching a stable level (still above the spontaneous firing rate) after about six to eight trials. The largest decrements were typically found for stimuli that caused the greatest initial response. A parallel decline during the session was seen for responses to the same stimuli presented as the matching item at the end of each trial. For the remaining neurons, there was either no change in response across the session or, infrequently (9%), a small increase in response. Because the number of cells responding strongly to an initially novel stimulus was smaller at the end of the session than at the beginning, there appears to be a focusing of activation within the population of cells as a result of experience.

The magnitude of the decrease in response to a given sample on a given trial depended on the number of intervening trials between successive presentations of the same sample. The decrement was much larger when only 4 trials intervened than when 35 trials intervened, although the cumulative decrement was retained even after 35 trials. Simple fatigue predicted the opposite, that is, greater decrements in response with the greater number of intervening trials, as the cells were activated on the intervening trials by many other stimuli. Thus, the cells could apparently detect that a specific stimulus had been presented before in the session, even after 4 to 35 intervening trials, or 16 to 140 intervening stimuli (given an average of four stimuli per trial). Consistent with this conclusion, when a few cells were retested with a new stimulus set, they showed a recovery of response on the initial presentation of the new stimuli. We do not yet know whether the decline in response to familiar stimuli is maintained for days (*10*).

Our results show that the responses of IT neurons to incoming visual stimuli carry information about the memories of past stimuli. The responses appear to be modulated according to the similarity of the stimulus to memory traces, whether the trace is actively held in short-term working memory or is passively held in a longer term store. The formation of memories may consist, at least in part, of the modification of synaptic weights such that familiar, expected, or recently seen stimuli cause the least activation of the cortex. This seemingly counterintuitive view is consistent with some neural network models of memory as well as with recent findings in humans and monkeys (*7, 11*). IT neurons may be acting as adaptive mnemonic filters that seek to preferentially pass information about new, unexpected, or not recently seen stimuli. Such a process would not simply precede memory storage but would be a critical component of the storage mechanism.

REFERENCES AND NOTES

1. M. Mishkin, *Philos. Trans. R. Soc. London* **85**, 95 (1982); J. A. Horel, M. L. Voytko, K. G. Salsbury, *Behav. Neurosci.* **98**, 310 (1984). One study that failed to find such an effect [D. Gaffan and L. Weiskrantz, *Brain Res.* **196**, 373 (1980)] may be explained as due to differences in the lesion site.
2. Electrode sites were localized on the anterior IT gyrus by magnetic resonance imaging.
3. Fixation was monitored with a magnetic search coil.
4. Because the monkey's reaction time was about 350 ms, only the first 275 ms of the neuronal response after stimulus onset were used in the analyses. Only correctly performed trials were counted, about 90% of the trials.
5. The stimuli used each day were chosen from a larger familiar set, and the animal saw the stimuli repeatedly before the recording began.
6. C. G. Gross *et al.*, *J. Neurophysiol.* **35**, 96 (1979); A. Mikami and K. Kubota, *Brain Res.* **182**, 65 (1980); G. C. Baylis and E. T. Rolls, *Exp. Brain Res.* **65**, 614 (1987); E. N. Eskandar *et al.*, *Invest. Ophthalmol. Vis. Sci. (Abstr.)* **32**, 1036 (1991); E. K. Miller, P. M. Gochin, C. G. Gross, *Vis. Neurosci.*, in press. In confirmation of other studies [J. M. Fuster and J. P. Jervey, *J. Neurosci.* **2**, 361 (1982); Y. Miyashita and H. S. Chang, *Nature* **331**, 68 (1988)], we sometimes found high maintained activity in the retention interval immediately after the sample presentation. The responses of neurons in area V4 are influenced by the cue given in a matching task, and it has been suggested that these effects are mediated by feedback from areas such as IT [P. E. Haenny, J. H. R. Maunsell, P. H. Schiller, *Exp. Brain Res.* **69**, 245 (1988)].
7. I. P. Riches *et al.*, *J. Neurosci.* **11**, 1763 (1991).
8. D. W. Hosmer and S. Lemeshow, *Applied Logistic Regression* (Wiley, New York, 1989).
9. We analyzed response changes over the session for each cell separately, using linear regression, evaluated at $P < 0.05$.
10. The responses of some face-selective cells in the superior temporal sulcus also decline in response to repetition of new faces [E. T. Rolls, G. C. Baylis, M. E. Hasselmo, V. Nalwa, *Exp. Brain Res.* **76**, 153 (1989)], and the responses of some neurons in area V4 habituate to repeated presentations of a grating within a trial [P. E. Haenny and P. H. Schiller, *ibid.* **69**, 225 (1988)]. Riches and co-workers (7) reported that some IT neurons respond better to novel than to familiar stimuli, but the time course of this effect was not clear.
11. T. Kohonen, *Self-Organization and Associative Memory* (Springer-Verlag, Berlin, 1984); G. A. Carpenter and S. Grossberg, *Neural Netw.* **3**, 129 (1990); L. R. Squire *et al.*, *Soc. Neurosci. Abstr.* **17**, 4 (1991).

12. We thank L. G. Ungerleider and M. Mishkin for valuable comments on the manuscript.

1 August 1991; accepted 3 October 1991

Lateral Movements of Membrane Glycoproteins Restricted by Dynamic Cytoplasmic Barriers

MICHAEL EDIDIN, SCOT C. KUO, MICHAEL P. SHEETZ*

Cell membranes often are patchy, composed of lateral domains. These domains may be formed by barriers within or on either side of the membrane bilayer. Major histocompatibility complex (MHC) class 1 molecules that were either transmembrane- (H-2D^b) or glycosylphosphatidylinositol (GPI)-anchored (Qa2) were labeled with antibody-coated gold particles and moved across the cell surface with a laser optical tweezers until they encountered a barrier, the barrier-free path length (BFP). At room temperature, the BFPs of Qa2 and H-2D^b were 1.7 ± 0.2 and 0.6 ± 0.1 (micrometers ± SEM), respectively. Barriers persisted at 34°C, although the BFP for both MHC molecules was fivefold greater at 34°C than at 23°C. This indicates that barriers to lateral movement are primarily on the cytoplasmic half of the membrane and are dynamic.

ALTHOUGH THE LATERAL DIFFUSION of a few membrane proteins, notably visual rhodopsin, is rapid and appears to be hindered only by the viscosity of membrane lipids, the lateral diffusion of most proteins is hindered in several ways. Significant fractions of most membrane proteins are immobile, and diffusion coefficients for the mobile fractions are 10- to 100-fold lower than that of rhodopsin (*1*). In erythrocyte membranes, the spectrin-actin complex limits the lateral diffusion of band 3 (micrometer scale) (*2*) but has little effect on rotation of band 3

M. Edidin, Department of Biology, The Johns Hopkins University, Baltimore, MD 21218.
S. C. Kuo and M. P. Sheetz, Department of Cell Biology, Duke University Medical Center, Durham, NC 27710.

*To whom correspondence should be addressed.

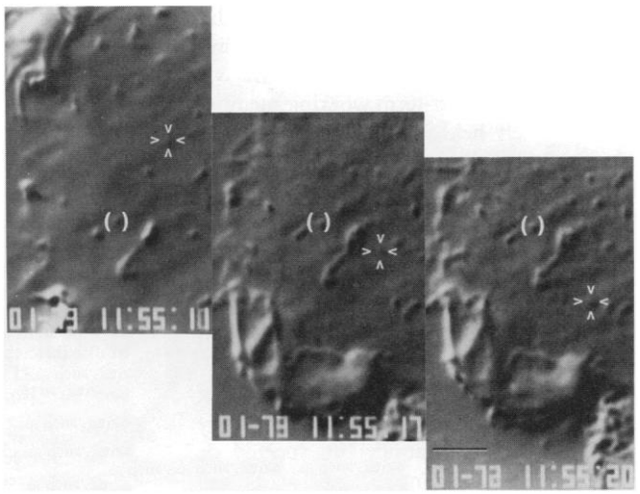

Fig. 1. Planar movement of a gold particle trapped by the laser optical tweezers. The gold particle was bound to the membrane by a monoclonal antibody (MAb) to Qa2, the GPI-linked protein, and was captured and moved laterally by the optical tweezers at a rate of 0.5 to 1 μm s^{-1}. The video overlay in each panel indicates time of day (hh:mm:ss), with the date portion monitoring a fraction of the laser power (in milliwatts). A stationary feature on the cell surface (marked by parentheses) was used to determine the relative distance the particle moved while in the optical trap (marked by carets). Murine HEPA-OVA cells were stably transfected with the Qa2 gene; the level of Qa2 expression was similar to that of the endogenous MHC class 1 molecule H-2D^b (*13*). Cells were plated on acid-washed cover slips (22 by 22 mm, No. 0) and cultured overnight in DME-FCS [Dulbecco's modified Eagle's medium (Gibco) with 10% fetal calf serum]. Gold particles (40 nm, E-Y Scientific) were mixed with an equal volume of MAb 20-8-4 (0.2 to 0.5 mg ml^{-1}) (*13*) in phosphate-buffered saline (PBS) (10 mM PO_4, 140 mM KCl, pH 7.4) and incubated for 10 min on ice before addition of dry bovine serum albumin (BSA) to a final concentration of 5 mg ml^{-1}. Particles were washed three times by centrifuging for 15 min at 6000*g* and resuspending the pellet in PBS with BSA (5 mg ml^{-1}); the final resuspended volume after washing was 10% of the original particle volume. Bath sonication was used to disrupt aggregates. Cells were washed with phenol red–free MEME (minimal essential medium with Earle's salts, Gibco) buffered by 10 mM Hepes (MEME-Hepes) and assembled in a flow-cell cover slip chamber that allowed exchanging the medium with a 1:9 dilution of the gold particle suspension in MEME-Hepes. Samples were maintained at 34°C by a hot-air incubator (constructed with the use of a plastic enclosure around the microscope optics with hot air supplied by a commercial hair dryer controlled with a Variac; a thermocouple in the enclosure monitored the temperature). The laser optical trap was constructed as described (*9*), but we substituted a 12-W laser (model 116F from Quantronix) to provide greater beam power. In the experiments, 15 to 30 mW of beam power was used at the sample. Scale bar = 2 μm.

(nanometer scale) (*3*). Thus, spectrin and associated proteins may form corrals partitioning the membrane (*4*). In this model, proteins move freely within a corral, on a scale of hundreds of nanometers, but only rarely cross the boundaries of corrals. Although the erythrocyte membrane is specialized and may be unusual, the model of constraints to lateral movement in its membrane may be used to explain anomalies in the lateral diffusion of other molecules, such as MHC class 1 molecules (*5*).

The properties of the MHC class 1 glycoproteins, H-2D^b and Qa2, are ideal for addressing the nature of restricted diffusion. Structurally, these two glycoprotein molecules are 80% homologous and have globular extracellular domains (*6*). However, the two proteins are anchored differently in the membrane: H-2D^b has a transmembrane segment and cytoplasmic tail, whereas Qa2 is anchored by a GPI linkage. Fluorescence photobleaching and recovery (FPR) measurements of lateral diffusion in the plasma membrane show different behaviors for these two molecules. The measurements are consistent with the notion that H-2D^b molecules are confined to domains approximately 1 μm in radius and Qa2 molecules are free to cross these boundaries (*5*). The mobile fraction, *R*, of H-2D^b molecules decreases with increasing size of the bleached spot, but the mobile fraction of Qa2 molecules remains constant (*5*). Because the diffusion coefficients for the mobile fraction of the two molecules are similar in small bleached areas, only the long-range diffusion of H-2D^b appears restricted. These data suggested that the cytoplasmic tail or transmembrane region, or both, encountered barriers in the cytoplasmic half of the membrane that were absent in the extracellular half. With the use of gold particle "handles" bound to these proteins by specific antibodies, we tested the barrier hypothesis by directly measuring the BFP for the two classes of MHC molecules by dragging them through the membrane with laser optical tweezers.

Membrane proteins tagged with gold or other particles provide a means to track the diffusional and directed movements of membrane glycoproteins. The diffusion coefficients, *D*, derived from single particle tracking have corresponded well with those measured by FPR (7). We measured $D = 1.3 \pm 0.2 \times 10^{-10}$ cm^2 s^{-1} (average ± SEM) for 26 particles attached to H-2D^b. For 23 particles attached to Qa2, $D = 2.1 \pm 0.3 \times 10^{-10}$ cm^2 s^{-1}. *D* from FPR measurements of diffusion over comparable areas (a fraction of a square micrometer) are 2×10^{-10} to 4×10^{-10} cm^2 s^{-1} for both kinds of MHC molecules (*5*).

The infrared laser tweezers can capture and move these gold-labeled MHC molecules. The mechanism of optically trapping such small particles (Rayleigh size range) has been described elsewhere (*8*). We positioned the beam waist of the laser trap such that gold particles free in solution were held in the plane of focus of the microscope when trapped (*9*). When subjected to viscous force in a flow cell, the trapped particle was always within a 0.5-μm radius until this viscous force exceeded the trapping force. As long as the membrane drag was less than the maximum force of the trap, particles dragged along the plane of the membrane remained in this radius (see Fig. 1). Moving the microscope stage at a rate of 0.5 to 1.0 μm s^{-1} kept the membrane drag minimal and yet allowed easy visualization of particles escaping the trap (>0.5 μm from center of trap) after encountering an obstacle. Under our experimental conditions (15 to 30 mW of infrared laser power at the sample), the maximum lateral force of the trap on the gold particles was <0.5 pN.

The BFP of each trapped particle was measured from video images, with stationary particles serving as reference points (Fig. 1). At room temperature (23°C), gold particles attached to H-2D^b molecules had a lower BFP than gold particles attached to Qa2 molecules. H-2D^b could be moved only 0.6 ± 0.1 μm (average ± SEM; number of determinations, $n = 68$) in any direction before being pulled from the trap. Particles attached to Qa2 molecules could be moved 1.7 ± 0.2 μm ($n = 53$). The maximum BFP of gold–H-2D^b was 3.5 μm, whereas the maximum BFP of gold-Qa2 was ~8 μm (Fig. 2, A and B). The statistical distribution of these BFP values appears exponential, but rigorous model testing was beyond the scope of this study.

The BFP of gold-labeled MHC molecules increased with increased temperature (34°C). However, the average BFP of the transmembrane-anchored H-2D^b molecules was still one-third the BFP of the GPI-anchored Qa2 molecules, 3.5 ± 0.6 μm ($n = 29$) for H-2D^b compared to 8.5 ± 0.8 μm ($n = 50$) for Qa2 (Fig. 2, C and D). These averages understate the differences between the two molecules. Particles on Qa2 molecules can be moved large distances on cells at 34°C. Seven out of 51 particles remained in the trap when the underlying surface was displaced a distance >15 μm. Ten other particles remained in the trap while the surface was displaced by >10 μm (Fig. 2, C and D).

Our earlier FPR measurements of membrane domains were made at 21°C (*5*). The results above implied that FPR at elevated temperatures should also detect membrane domains and that these domains would appear larger than at room temperature. This was indeed the case (Fig. 3). The mobile fraction of labeled H-2D^b molecules was higher at 37°C (R = 0.7) than at room temperature [R = 0.5; see (*5*) for the range of values at room temperature] and decreased when the size of the bleached spot was increased (Fig. 3, A and B). The mobile fraction of Qa2, which was also higher at 37°C than at room temperature, did not change when the size of the bleached spot was increased (Fig. 3, C and D).

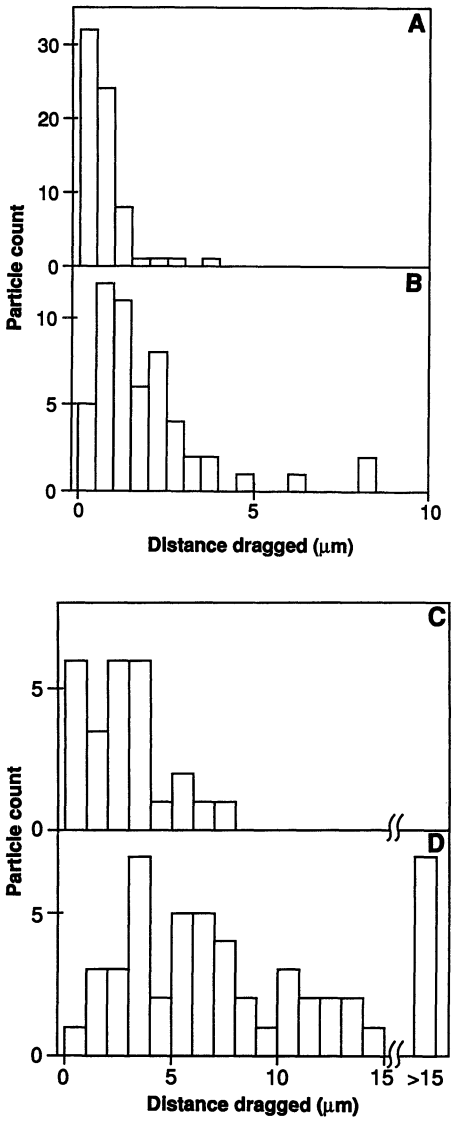

Fig. 2. Distance traveled at 23°C by 40-nm gold particles attached to MHC molecules on HEPA-OVA cells. Measurements were made as described in Fig. 1: (**A**) H-2D^b molecules bound to MAb 28-14-8 (*14*) labeled with gold particles. (**B**) Qa2 molecules detected with gold-labeled MAb 20-8-4 (*15*). Distance traveled at 34°C by 40-nm gold particles attached to MHC molecules: (**C**) H-2D^b molecules. (**D**) Qa2 molecules.

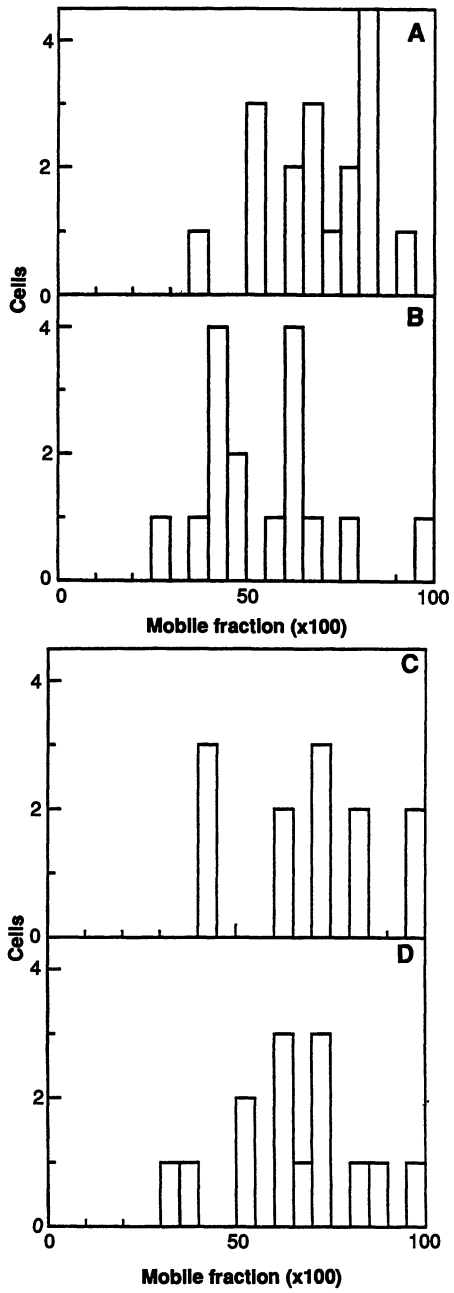

Fig. 3. FPR measurements of the mobile fractions, R, of MHC molecules labeled at 37°C with fluorescent adducts of the same Fab fragments that were used for BFP measurements, MAb 28-14-8 for H-2D^b and MAb 20-8-4 for Qa2. On the same day, measurements of D were made at, 22°C with a laser spot size of 0.65 μm: D = 13 ± 2 × 10^{-10} cm^2 s^{-1} (n = 15) for H-2D^b and D = 13 ± 2 × 10^{-10} cm^2 s^{-1} (n = 22) for Qa2. The difference between these values and previous values (*5*) is most likely due to the smaller number of observations. There was no significant increase in D with a 15°C increase in temperature. (**A**) H-2D^b. Radius of the laser spot, 0.65 μm; mobile fraction, 0.70 ± 0.04 (mean ± SEM); D = 5.6 ± 1 × 10^{-10} cm^2 s^{-1} (n = 16). (**B**) H-2D^b. Radius of the laser spot, 1.1 μm; mobile fraction, 0.55 ± 0.04 (mean ± SEM); D = 16 ± 4 × 10^{-10} cm^2 s^{-1} (n = 15). (**C**) Qa2. Radius of the laser spot, 0.65 μm; mobile fraction, 0.70 ± 0.06 (mean ± SEM); D = 11 ± 2 × 10^{-10} cm^2 s^{-1} (n = 12). (**D**) Qa2. Radius of the laser spot, 1.1 μm; mobile fraction, 0.71 ± 0.06 (mean ± SEM); D = 32 ± 6 × 10^{-10} cm^2 s^{-1} (n = 12).

Both laser trapping and FPR experiments indicate that there are barriers to lateral movements of MHC molecules. Both methods also show that the GPI-anchored Qa2 molecules encounter barriers less frequently than do H-2D^b molecules. The major difference between the two types of molecules is that H-2D^b molecules extend completely through the membrane bilayer and bear a cytoplasmic tail (*6*).

These structural data suggest a model for the more limited lateral mobility of H-2D^b molecules. These molecules collide with a cellular structure underlying or within the cytoplasmic half of the membrane, a membrane-associated cytoskeleton. Interactions with lipid domains or other transmembrane proteins anchored to a cytoskeleton are discounted because they should also affect Qa2 mobility. However, the extent of lateral mobility of Qa2 molecules is likely to be limited by collisions with other membrane glycoproteins that are either corralled or anchored to a cytoskeleton. The barriers to lateral displacement we observe cannot account for the decreased diffusion coefficients of glycoproteins in biological membranes (*1*). This is evident when we compare the fivefold increase in BFP that accompanies an 11°C increase in temperature with the small change in D observed for the same increase in temperature (see caption of Fig. 3).

The barriers on the cytoplasmic half of the membrane are likely to contain spectrin and its membrane anchor ankyrin. Spectrin and ankyrin are major constituents of the erythrocyte membrane skeleton and occur in many other cell types as well (*10*). Barriers composed of a perfect spectrin mesh, 0.2 μm on a side, would create smaller domains than implied by our work. However, larger values of BFP do not necessarily imply larger distances between elements of a stable cytoskeletal meshwork. Rather, the BFP could reflect the probability of encountering a stationary element of a dynamic and changing mesh whose characteristic dimensions are smaller than the BFP. Such a metabolically active membrane skeleton, with transient breaks in the meshwork, would be indistinguishable from an intact, stable meshwork of larger dimensions. The increased BFP of particles at 34°C compared to 23°C is not consistent with an inert web of barriers. A dynamic, hence imperfect, matrix of spectrin could regulate both short-range (*11*) and long-range (*12*) molecular interactions on the cell surface.

REFERENCES AND NOTES

1. K. Jacobson, A. Ishihara, R. Inman, *Annu. Rev. Physiol.* **49**, 163 (1987); M. Edidin, in *The Structure of Cell Membranes*, P. Yeagle, Ed. (CRC Press, Boca Raton, FL, in press).

2. M. P. Sheetz, M. Schindler, D. E. Koppel, *Nature* **285**, 510 (1980).
3. E. A. Nigg and R. J. Cherry, *Proc. Natl. Acad. Sci. U.S.A.* **77**, 4702 (1980).
4. M. P. Sheetz, *Semin. Hematol.* **20**, 175 (1983).
5. M. Edidin and I. Stroynowski, *J. Cell Biol.* **112**, 1143 (1991).
6. I. Stroynowski, *Annu. Rev. Immunol.* **8**, 501 (1990).
7. M. P. Sheetz, S. Turney, H. Qian, E. L. Elson, *Nature* **340**, 284 (1989); R. N. Ghosh and W. W. Webb, *Biophys. J.* **57**, 286a (1990); M. de Brabander *et al.*, *J. Cell Biol.* **112**, 111 (1991).
8. A. Ashkin, J. M. Dziedzic, J. E. Bjorkholm, S. Chu, *Opt. Lett.* **11**, 288 (1986); S. M. Block, in *Noninvasive Techniques in Cell Biology*, J. K. Foskett and S. Grinstein, Eds. (Wiley-Liss, New York, 1990), pp. 375–402.
9. D. Kucik, S. C. Kuo, E. L. Elson, M. P. Sheetz, *J. Cell Biol.* **114**, 1029 (1991).
10. G. V. Bennett, *Curr. Opin. Cell Biol.* **2**, 51 (1990).
11. R. Peters, *FEBS Lett.* **234**, 1 (1988).
12. M. Saxton, *Biophys. J.* **58**, 1303 (1990).
13. I. Stroynowski, M. Soloski, M. G. Low, L. E. Hood, *Cell* **50**, 759 (1987).
14. K. Ozato and D. Sachs, *J. Immunol.* **125**, 2473 (1980).
15. ———, *ibid.* **126**, 317 (1980).
16. Supported by NIH grants AI14584 (to M.E.) and GM 36277 (to M.P.S.), a grant from the Muscular Dystrophy Association (to M.P.S.), and a grant from the Jane Coffin Childs Memorial Fund for Medical Research (to S.C.K.).

5 August 1991; accepted 7 October 1991

Identification of a Competitive HGF Antagonist Encoded by an Alternative Transcript

ANDREW M.-L. CHAN, JEFFREY S. RUBIN, DONALD P. BOTTARO, DAVID W. HIRSCHFIELD, MARCIO CHEDID, STUART A. AARONSON*

We identified a naturally occurring hepatocyte growth factor (HGF) variant, whose predicted sequence extends only through the second kringle domain of this plasminogen-related molecule. This smaller molecule, derived from an alternative HGF transcript, lacked mitogenic activity but specifically inhibited HGF-induced mitogenesis. Cross-linking studies demonstrated that the truncated molecule competes with HGF for binding to the HGF receptor, which has been identified as the c-*met* proto-oncogene product. Thus, the same gene encodes both a growth factor and its direct antagonist.

HGF WAS INITIALLY DETECTED AS A hormone-like activity capable of stimulating hepatocyte proliferation (*1*). This growth factor is expressed by stromal fibroblasts and is mitogenic for a variety of cell types, including melanocytes, endothelial cells, and cells of epithelial origin (*2*). HGF is also highly related or identical to scatter factor, an agent that stimulates the dispersion of epithelial and vascular endothelial cells (*3*). Studies have identified the HGF receptor as the c-*met* proto-oncogene product (*4*), a membrane-spanning tyrosine kinase (*5*). Structurally, HGF resembles plasminogen in that HGF has characteristic NH_2-terminal kringle domains (*6*) and a COOH-terminal serine protease–like domain (*7, 8*). HGF is synthesized as an 87-kD single chain polypeptide (p87). Like plasminogen, it can be cleaved into a heterodimeric form consisting of a heavy (~60 kD) and a light chain (~30 kD) held together by disulfide bonds (*1*).

We have reported that human fibroblasts in culture secrete HGF p87 as the predominant form of the growth factor (*2*). Survey of a number of HGF-producing cell lines confirmed that p87 was the major secreted product among the various HGF species. However, we also detected variable amounts of lower molecular mass HGF-immunoreactive species by using SDS–polyacrylamide gel electrophoresis (PAGE) under reducing conditions. When similar experiments were performed under nonreducing conditions to prevent dissociation of any HGF heterodimers, we observed the high molecular mass HGF species, as well as lesser amounts of a 28-kD (p28) HGF-immunoreactive polypeptide. The concentration of p28 in medium from the SK-LMS-1 line (*9*) was striking (Fig. 1A). These results, as well as pulse-chase experiments (*10*), suggested that p28 was not derived from p87 but represented instead an independently synthesized HGF-immunoreactive protein.

To identify the transcript that encoded the p28 protein, we performed Northern (RNA) blot analysis with polyadenylated [poly(A)$^+$] RNA prepared from SK-LMS-1 cells. When the full-length HGF coding sequence was used as a probe, two major transcripts of 6.0 and 3.0 kb were detected (Fig. 1B) that encode the full-length growth factor (*2*). In addition, we detected an HGF RNA species of ~1.3 kb. The three transcripts were observed in normal placenta, as well as in fibroblasts derived from different tissues. However, the ratios of the transcripts showed considerable variation, with foreskin fibroblasts expressing the highest relative amount of the 1.3-kb message (Fig. 1B). Because only a portion of the 2.2-kb HGF coding sequence could be present in the small transcript, we reasoned that it might encode p28. To better define this transcript, we carried out Northern analysis with poly(A)$^+$ RNA from M426 human embryonic lung fibroblasts, separately hybridized with probes derived from either the HGF NH_2-terminal heavy chain (H) or the COOH-terminal light chain (L) regions. Whereas both probes detected the 6.0- and 3.0-kb transcripts, only the H probe was capable of recognizing the 1.3-kb message (Fig. 1B). These results suggested that this RNA species encoded a truncated version of the HGF molecule that contained sequences specific to its NH_2-terminal region.

To isolate cDNA corresponding to the 1.3-kb transcript, we differentially screened an M426 cDNA library (*11*) with both HGF H and L probes. Clones that specifically hybridized to the H probe were plaque purified. On the basis of sizes and physical maps of the inserts, we selected one 1.2-kb cDNA clone, pH45, for sequencing. The 1199-bp cDNA contained a short 5′ untranslated region of 75 bp, an open reading frame of 870 bp, and a 254-bp 3′ untranslated region containing a polyadenylation signal, AATAAA (Fig. 2A). The open reading frame predicted a 290–amino acid truncated version of HGF consisting of a signal peptide (S), an NH_2-terminal domain (N), and the first two kringle domains (K1 and K2) with a calculated size of ~30 kD, excluding the signal peptide. This sequence, designated HGF/NK2 (*11a*), was identical to that of HGF cDNA, including the 5′ untranslated region, until it diverged precisely at the end of the K2 domain. The HGF/NK2 open reading frame continued for two additional amino acids, followed by an in-frame stop codon (TAA). These findings suggested that HGF and HGF/NK2 cDNAs were derived from alternative transcripts of the HGF gene.

To define the splicing event that generated the truncated cDNA, we used the polymerase chain reaction (PCR) with primers P1 and P2 (Fig. 2A) to amplify specific HGF/NK2 sequences. Whereas the reaction yielded the expected 227-bp PCR product with HGF/NK2 cDNA, a ~600-bp fragment was detected when human genomic DNA was used as template. Sequencing of the latter PCR product revealed a ~400-bp intron flanked by consensus splice donor/acceptor sequences, CG/GT and AG/AG, at the intron-exon boundaries. These aligned precisely with the predicted splice junction in the HGF/NK2 cDNA clone (Fig. 2B).

Laboratory of Cellular and Molecular Biology, National Cancer Institute, Bethesda, MD 20892.

*To whom correspondence should be addressed.